RevMexAA (Serie de Conferencias), **2**, 97-104 (1995)

THE CARINA NEBULA IN X-RAYS

M.F. Corcoran[1,2], J. Swank[2], G. Rawley[3], R. Petre[2], J. Schmitt[4], and C. Day[1,2]

RESUMEN

Se usan nuevas observaciones *ROSAT* PSPC y HRI de la región de la Nebulosa de Carina para examinar la emisión de rayos X provenientes de las fuentes discretas y también del gas caliente difuso en la nebulosa cerca de η Car. La mayor parte de la emisión difusa viene de gas a temperatura de unos pocos millones de grados, pero también se detecta gas difuso más caliente (4×10^7 K) en una región de 11 pc alrededor de η Car. η Car muestra un espectro de 3 componentes con temperaturas de 10^6, 6×10^6 y 4×10^7 K. Se ha resuelto con el HRI una capa de gas 0.1×0.2 pc alrededor de η Car, que emite en rayos X y, de la comparación de las imágenes *Einstein* HRI and *ROSAT* HRI, se sugiere que las componentes blandas se originan en la capa (la cual no es resuelta por el PSPC) mientras que el gas más caliente se produce a menos de 1″ de la estrella óptica. Los espectros de las estrellas O brillantes están caracterizados por dos componentes de temperatura (10^7 y 2×10^6 K) y generalmente muestran columnas de absorción más grandes que la columna interestelar. Se usan observaciones PSPC y *ROSAT* HRI para examinar la relación L_X/L_{bol} para estrellas calientes de la clase espectral B-temprana en el campo.

ABSTRACT

New *ROSAT* PSPC and HRI observations of the Carina Nebula region are used to examine the X-ray emission from the discrete sources as well as the diffuse hot gas in the Carina Nebula near η Carina. Most of the diffuse emission comes from gas at a temperature of a few million degrees, but hotter (4×10^7 K) diffuse gas in an 11 pc region around η Car is also detected. η Car shows a 3 component spectrum with temperatures of 10^6, 6×10^6 and 4×10^7 K. A 0.1×0.2 pc shell of X-ray emitting gas around η Car has been resolved by the HRI, and comparison of the *Einstein* HRI and *ROSAT* HRI images supports the suggestion that the soft components originate in the shell (which is unresolved by the PSPC) while the hottest gas is produced less than an arcsec from the optical star. Spectra of the bright O stars are characterized by 2 temperature components (10^7 K and 2×10^6 K) and generally show absorption columns larger than the interstellar column. PSPC and *ROSAT* HRI observations are used to examine the L_X/L_{bol} relation for hot stars in the field through the early-B spectral class.

Key words: **ISM: INDIVIDUAL OBJECTS: (η CAR) — STARS: EARLY-TYPE — X-RAY: SOURCES**

[1] USRA, Code 668, Goddard Space Flight Center, Greenbelt, MD 20771, USA.
[2] LHEA, Code 666, Goddard Space Flight Center, Greenbelt, MD 20771, USA.
[3] Applied Research Corporation, 8201 Corporate Dr., Landover, MD 20785, USA.
[4] MPE, 8046 Garching bei Munchen, Germany.

1. INTRODUCTION

The Carina Nebula region is one of the most interesting massive star forming regions of the Galaxy, containing bright nebulosities, faint dust lanes, open clusters with dozens of massive hot stars in various evolutionary stages (including 6 O3 stars and 3 Wolf-Rayet stars), and the peculiar object η Car. η Car is surrounded by a nebulosity called the homunculus which apparently was ejected from the star during an eruptive event in the 1840s. The nature of η Car is unknown but the star is generally thought to be a single very massive star close to the Humphreys-Davidson instability limit (Davidson 1971) although binary and multiple-star scenarios have also been proposed (Warren-Smith et al. 1979).

Observations of the Carina Nebula region with early non-imaging X-ray detectors (*OSO-8*, Becker et al. 1976; *Uhuru*, Forman et al. 1978) revealed at least one source of X-rays, and indicated the presence of a hard component at a temperature of a few keV. Observations with the imaging instruments on the *Einstein* Observatory (Seward et al. 1979; Seward & Chlebowski 1982; Chlebowski et al. 1984) showed various contributors to the X-ray flux: point source emission from the hot stars, point source and extended emission from η Car, and soft emission from a diffuse component generally associated with the optical nebulosities. The diffuse emission and the emission from most of the hot stars is produced by a thermal plasma of temperature near 1 keV. η Car however showed a complex, multi-temperature spectrum. Spectra of η Car obtained with the IPC and the SSS (Chlebowski et al. 1984) detected thermal emission at temperatures of a few hundred eV and 4 keV, which indicated that at least some of the high temperature emission observed by *OSO-8* and *Uhuru* originated very near η Car. A more recent *Ginga* observation (Koyama et al. 1990) of the Carina Nebula region determined a temperature for the hot gas of 4.1 keV, while a comparison of the *Ginga* and SSS fluxes suggested that some of the hot emission originated over an extended region of a few tenths of a degree in size. The Carina Nebula was also the target of a BBXRT pointing, which provided the first moderate resolution measure of the iron line region.

2. THE *ROSAT* OBSERVATIONS

The Carina Nebula was observed by both the PSPC and the HRI on *ROSAT*. The PSPC observations took place in June and December 1992 for a total of 37 ksec. The HRI observation in hand consists of a 12 ksec observation obtained in July 92. Another 38 ksec of HRI time awaits scheduling and processing. The purpose of these observations was to determine temperature variations in the diffuse emission, to determine the extent of the 4 keV component, to examine the X-ray luminosity function of the hot stars and look for variability in the point sources, and to resolve the extent and spectral distribution of the hot gas in and around η Car. The PSPC greyscale image is shown in Figure 1.

3. ANALYSIS OF THE DIFFUSE EMISSION

We extracted spectra from 7 regions within the diffuse emission indicated in Fig. 1. We used the spectrum from region 8 (which is outside most of the diffuse emission) as a measure of the background (a combination of scattered solar X-rays, charged particles and cosmic background not associated with the Carina nebula). We modeled the spectrum from region 8 and included this model as a fixed background component in our spectral modeling of the other 7 regions. Derived temperatures, columns and emission measures are given in Table 1. The average number density is $n = \sqrt{EM/V}$, where EM is the emission measure and V is the volume of the hot gas. Because we do not know the depth of the hot gas along the line of sight, the volume of the hot gas is not known and thus we cannot determine the density of the hot gas accurately. In order to crudely estimate densities, we assumed that the hot gas uniformly filled the volume obtained by revolving the spectral extraction region (which was either a circular or elliptical region) around one axis. The derived densities are given in Table 1.

Most regions were adequately fit by 1 temperature models with a temperature of a few million degrees. An exception to this is region 7, a 7 arcmin radius circle centered near η Car (which excluded η Car, HD 93162, HD 93204 and HD 93205) which required an additional hot component with $T \approx 4.1 \times 10^7$ K. Thus the PSPC indicates the presence of very hot gas in an extended region of radius at least 7 arcmin (11 pc at the distance of the Carina Nebula, taken as 2600 pc). However, the surface brightness we derive by extrapolating the *ROSAT* spectrum into the 2-10 keV *Ginga* band is 9.3×10^{14} ergs s^{-1} cm^{-2} arcmin^{-2} which is almost a factor of 2 smaller than the *Ginga* value (1.6×10^{13} ergs s^{-1} cm^{-2} arcmin^{-2}). This discrepancy may be due in part to uncertainties in the extrapolation of the *ROSAT* spectrum to the *Ginga* bandpass. Alternatively it may indicate that other regions of high temperature gas exist beyond the vicinity of η Car.

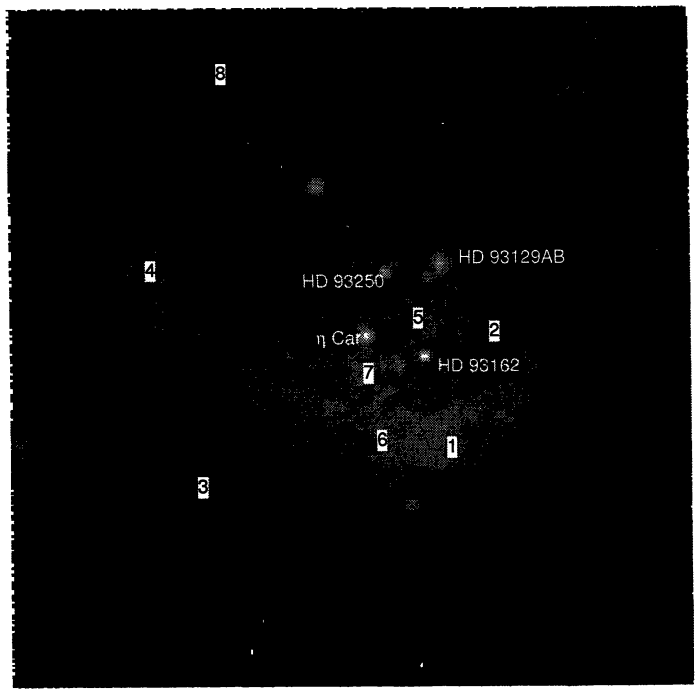

Fig. 1. PSPC image of η Car. North is to the top, east to the left. Several bright stars and diffuse emission are apparent. Bright stars and regions of diffuse emission used in the spectral analysis are marked.

Table 1. Analysis of Diffuse Emission Spectra

#	N_H (10^{22} cm^{-2})	Log(T) (K)	Log(EM) (cm^{-3})	Density (cm^{-3})	Surface Brightness cgs	χ^2/Nbins
1	0.26	6.62	56.82	0.66	1.38E-13	57/33
2	0.45	6.37	56.85	0.90	3.11E-14	28/33
3	0.64	6.21	58.11	2.67	4.61E-14	31/33
4	0.63	6.43	57.32	1.08	4.94E-14	43/33
5	0.76	6.21	57.94	7.17	8.02E-14	46/34
6	0.20	6.62	56.18	0.72	9.97E-14	35/33
7	0.56	6.43	58.08	0.62	9.59E-14	219/33
2 Temperature Fits						
7	0.20	7.65	56.66	0.12	1.05E-13	37/33
	0.21	6.58	57.19	0.14		
1	0.24	6.91	55.63	0.17	1.39E-13	55/33
	0.20	6.63	56.67	0.16		
Total	0.54	6.93	57.27	0.01	7.20E-14	69/31
	0.20	6.50	57.73	0.04		

4. X-RAY EMISSION FROM η CAR

4.1. The Broad-Band X-ray Spectrum of η Car

The *Einstein* SSS spectrum of a region centered on η Car by Chlebowski et al. was fit by at least 2 thermal components, a soft, unabsorbed component ($T = 4 \times 10^6$ K, $N_H = 2 \times 10^{21}$ cm^{-2}) and a hard, absorbed component ($T \approx 8 \times 10^7$ K, $N_H = 5 \times 10^{22}$ cm^{-2}). Observations with non-imaging detectors (*OSO-8*, MPC,

Ginga) also detected the presence of Fe K-line emission near 7 keV. We used our PSPC data in conjunction with other publically available observations at higher energies to examine the nature of the X-ray spectrum from η Car and the origin of the Fe line emission. We extracted a spectrum in a 2 arcmin radius circle around η Car from the PSPC observation. We extracted a background spectrum in a 2 arcmin annulus centered around η Car, excluding less luminous point sources which happened to fall in the extraction region. In order to extend the bandpass to higher energies, we also extracted source and background spectra from a public-domain IPC observation (sequence number 776) using the same source and background regions. We also examined the spectrum of the η Car region as observed by the SSS, in the hopes of providing improved spectral resolution. However, we found that we were unable to simultaneously fit the SSS and net PSPC and IPC spectra. This is most likely due to the contamination of the SSS spectrum by the X-ray background around η Car which fell within the 6 arcmin diameter field-of-view of the SSS. An estimate of the background contamination in the SSS field-of-view could be made from the IPC data, as was done by Chlebowski et al. in their analysis. We preferred to take a different, complementary approach. We used the background-corrected PSPC spectrum and the background-corrected IPC spectrum to define the source spectrum from $0.1 - 4.5$ keV, the combined PSPC-IPC energy bands. We then used the BBXRT spectrum of η Car to define the high energy ($E \geq 4$ keV) part of the spectrum and to provide a moderately-resolved spectrum of the Fe line region near 7 keV. Because BBXRT had only crude imaging capabilities, no real background correction could be made for these data; however, the diffuse background makes its greatest contribution at low energies ($E \leq 3$ keV); at higher energies the contribution due to the diffuse background is less important. Thus, by restricting the BBXRT spectrum to the energy range ≥ 3 keV, we were in effect able to exclude most of the diffuse background. This seemed a satisfactory compromise, since the net IPC spectrum, which covers from 0.44.5 keV, nicely bridges the PSPC band ($0.2 - 2.4$ keV) and the (truncated) BBXRT band ($3.0 - 10$ keV) and serves as a check on the importance of background contamination in the BBXRT spectrum.

We performed a simultaneous fit to the PSPC, IPC and truncated BBXRT spectrum using absorbed Raymond-Smith thermal spectra as the input model. Our best fit to the data required 3 thermal components, yielding a value of $\chi^2 = 110$ for 63 degrees of freedom. The derived parameters are given in Table 2 below, while the best fit spectrum (deconvolved from the detector responses) is shown in Figure 2. The values of N_H below do not include the contribution from the ISM, which was fixed at 2×10^{21} cm^{-2}. The unabsorbed luminosity for this model is Log $L_X = 35.55$, which is somewhat larger than the value derived by Chlebowski et al., Log $L_X = 34.40$, mainly due to the larger value of N_H which we derive for the hottest component. Our X-ray luminosity implies Log $L_X/L_{bol} = 5.1$. This is a much higher L_X/L_{bol} ratio than is obtained for any of the other point sources in the field (see § 5.1 below).

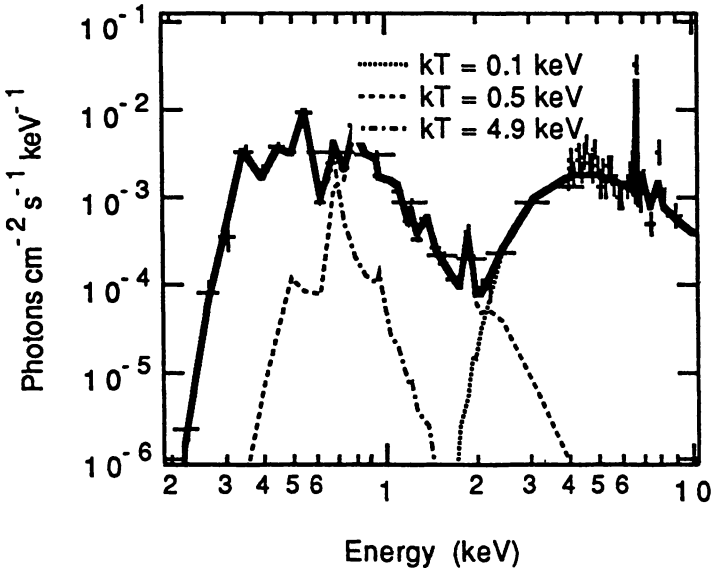

Fig. 2. η Car 0.2-10 keV spectrum from PSPC, IPC and BBXRT observations

Table 2. Best fit to Composite η Car Spectrum

Log (T)	Log(EM)	Log(N_H)
7.75	58.24	23.20
6.77	56.60	21.48
6.06	57.26	...

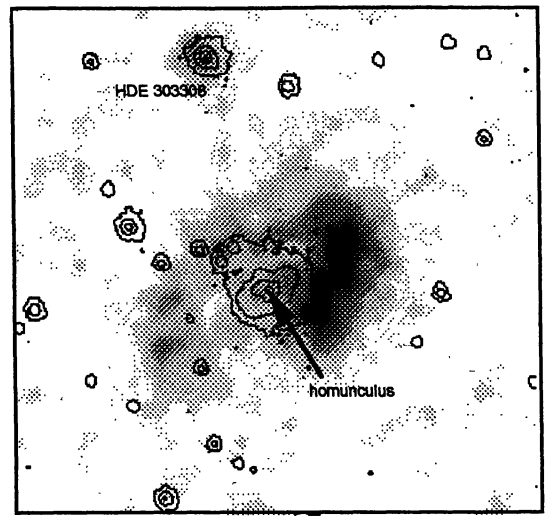

Fig. 3. *ROSAT* HRI map of η Car and optical image of homunculus. The bright source to the northeast of the homunculus is HDE 303308 which is about 1 arcmin from η Car.

4.2. Extended Emission

A 15 × 20 arcsec (0.2 × 0.3 pc) shell of X-ray emitting gas surrounding the homunculus was imaged by both the *Einstein* and *ROSAT* HRI. Figure 3 shows the *ROSAT* HRI image including optical contours of the homunculus. The X-ray shell is aligned with the axes of symmetry of the homunculus. Analysis of the η Car PSPC spectrum (which includes the emission from the extended shell) indicates the presence of soft components with temperatures of 1 and 6 million degrees as well as a much hotter, highly absorbed component with a temperature near 45 million degrees. If the soft emission originates in the extended shell, then the velocities implied by the X-ray temperatures are about 200 km s^{-1}. If the hot gas was ejected from η Car, the velocity and extent of the gas imply that the gas was ejected more than 100 years ago. Assuming that the hot gas forms an elliptical shell with semi-major axes of 0.10 × 0.10 × 0.12 pc and a thickness of 0.02 pc, the density of the shell is 157 cm^{-3} and the total mass of hot gas in the shell is 0.01 solar mass. Figure 4 shows a comparison of the *Einstein* and *ROSAT* HRI images. A point source of emission at the position of the optical center of light of η Car is apparent in the *Einstein* image but not in the *ROSAT* HRI image. This is consistent with the suggestion made by Chlebowski et al. of the existence of a hard absorbed source less than an arcsec from the location of η Car. Because the source is hard ($T \approx 4$ keV) and absorbed ($N_H \approx 10^{22}$ cm^{-2}) it is not visible in the *ROSAT* band, which cuts off at about 2.4 keV. However, this hard source is detectable by *Einstein* HRI since the *Einstein* bandpass extends to 4.5 keV.

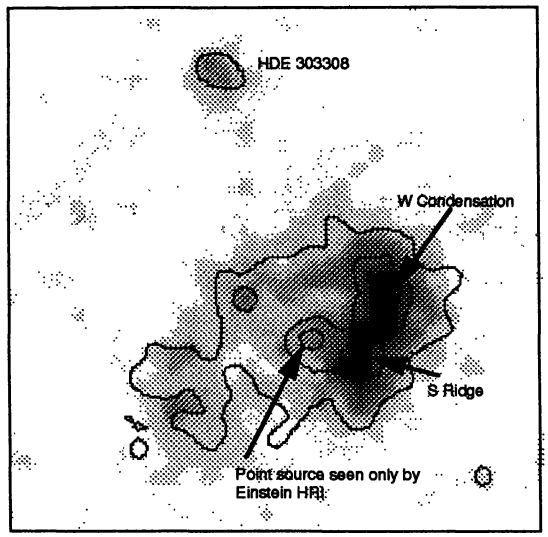

Fig. 4. *ROSAT* (greyscale) and *Einstein* (contours) HRI maps of η Car. The S and W condensations are sources of soft X-rays visible in both maps. The X-ray point source at the optical center of the homunculus is hard and only visible in the *Einstein* map.

5. OTHER POINT SOURCES

5.1. The X-ray Luminosity Function

We derived counting rates for all known sources in the field of the PSPC image using the maximum-likelihood technique described by Pollock (1987). A 3 × 3 arcmin sub-image centered on the position of each known source was extracted from the PSPC image. The maximum likelihood technique then determines the likelihood that a point source is present above background, and if so, gives the most likely number of source and background counts in the sub-image. Source counting rates were determined by dividing the most likely number of source counts by the average value of the exposure time in the appropriate 3 × 3 arcmin sub-section of the merged exposure map. Positions of optical sources were obtained from the list of SIMBAD sources provided as a standard *ROSAT* data product. Positions from the SIMBAD list were also checked with source positions from Seward & Chlebowski (1982) for consistency.

We found that the PSPC detected more than 20 stars as X-ray sources at or above the 3σ level. The 5 brightest sources (excluding η Car) in the PSPC image are listed in Table 3, along with their maximum-likelihood counting rates and derived 2σ errors. We extracted spectra for the 5 brightest sources listed in Table 3 (§ 5.3) and derived unabsorbed luminosities for all these sources and determined an energy conversion factor of $8.9(\pm1) \times 10^{11}$ ergs cm^{-2} count^{-1} for these 5 stars. Assuming that the spectra from the fainter detected sources are similar to the brightest sources, we used this energy conversion factor to convert from PSPC count rates to unabsorbed luminosities for the fainter sources. Figure 5 shows our derived correlation between bolometric luminosity and X-ray luminosity. In general we found that $L_X/L_{bol} \approx 2 \times 10^{-7}$, which is similar to the result obtained by Seward & Chlebowski (1982). There are some noticeable exceptions to this relation. η Car has the largest L_X/L_{bol} of any star in our sample. We confirm the "overluminous" nature of the WR star HD 93162 which was first noted by Seward & Chlebowski; for HD 93162, we find that $L_X/L_{bol} \approx 2 \times 10^{-6}$, similar to the value previously obtained. In addition, the PSPC observation also detected a group of X-ray bright B stars with L_X/L_{bol} = a few $\times 10^{-6}$, which were not visible in the IPC pointings. However, we should point out that spectroscopic classification (and hence bolometric luminosities) are more uncertain for these stars than for the brighter stars.

5.2. X-ray Variability

X-ray lightcurves were extracted from the PSPC observation for all the stars listed in Table 2, and for η Car as well. No significant variability was detected in any of the bright sources at above the 10% level.

Table 3. Spectral Analysis of the Bright Stars

Star	Spectral Type	PSPC rate cts s^{-1}	N_H 10^{22} cm^{-2}	Log(T) K	Log(EM) cm^{-2}	$\chi^2\nu$ (2T)	$\chi^2\nu^a$ (1T)	Log(L_X)^b (ergs s^{-1})
HD 93250	O3V	0.070±0.005	0.21	7.20	56.14			
			0.32	6.57	56.09	0.93	3.2	33.45
HD 93129AB	O3I + O3V	0.093±0.006	0.30	7.67	56.58			
			0.20	6.89	55.84	1.04	4.7	33.69
HD 93162	WN7+abs	0.288±0.007	0.41	7.30	56.73			
			0.42	6.91	56.00	1.48	1.9	33.76
HD 93403	O5III	0.054±0.005	0.36	7.64	56.19			
			0.22	6.96	55.85	0.96	1.8	33.32
HD 93205	O3V + O8	0.053±0.004	1.47	7.29	56.30			
			0.20	6.39	55.89	1.44	2.1	33.43

[a] Reduced χ^2 of best single temperature Raymond-Smith fit.
[b] L_X has been corrected for ISM + circumstellar absorption, and is in the range 0.2 − 2.4 keV.

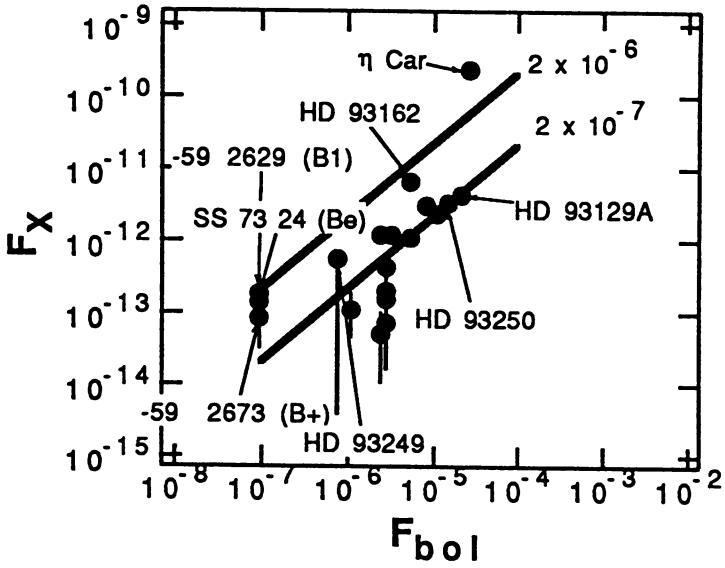

Fig. 5. Dependence of L_X on L_{bol} for detected stars.

5.3. X-ray Spectral Modeling

X-ray spectra were extracted for the 5 sources (not including η Car) having more than 500 counts. Source spectra were extracted in a circular region of about 2 arcmin radius centered on the source. Background spectra were in general extracted in an annulus around the source region. Serendipitous sources in the source and background extraction regions were excluded. We fit each net spectrum with absorbed 1 and 2 temperature Raymond-Smith type spectra. In general, we found that net spectra with more than about 1000 counts were not adequately fit by single-temperature thermal models. The addition of another absorbed component generally was required to provide an adequate fit, and in the case of HD 93162 and HD 93205 a 2 component fit did not provide a good description of the data (although the 2 component fit yielded a lower value of reduced χ^2 than a single component model in these cases). Results of the spectral modeling are summarized in Table 3. We typically found temperatures of a few 10^7 K and a few 10^6 K, with absorbing columns for both the hot and

cool components near but somewhat larger than the interstellar value of 2×10^{21} cm^{-2}. HD 93205 showed an exceptionally large column of 1.5×10^{22} cm^{-2} toward the hot component, but this parameter is only loosely constrained and the 1σ lower bound on this parameter is less than 5×10^{21} cm^{-2} which is not significantly larger than the columns found for the other 4 stars in the sample. We did not find any significant correlation between mass loss rate, wind terminal velocity or wind momentum flux and the parameters (temperature, column or emission measure) of the hot gas.

6. SUMMARY

There are many distinct components which contribute to the X-ray emission from the Carina Nebula: point-source emission from the hot stars, diffuse emission produced by hot gas spread throughout the nebula, and emission from η Car itself. The observed X-ray emission suggests the action of shock heating on a wide variety of spatial scales.

The point source emission associated with the early-type stars represents the process of shock heating on the smallest available scales, a few $\times 10^{11}$ cm, since X-rays from early-type stars are generally attributed to shock-heating caused by instabilities in the radiatively-driven winds not too far from the stellar photosphere. On a larger scale ($10^{18} - 10^{20}$ cm), the diffuse X-ray background which permeates this region is probably produced as large volumes of gas are driven into the surrounding ISM by the combined action of the OB + WR stellar winds. The X-ray temperatures we derive for this gas, a few million degrees K, correspond to shock velocities of a few hundred km s^{-1}, which is in good agreement with measured velocities of interstellar line complexes in the nebula. On an intermediate scale, η Car shows both highly localized, high temperature emission and extended, cooler emission. The soft emission is seen on scales up to a few 10^{16} cm and is produced by as relatively slow moving material ejected from the star interacts with the circumnebular material; while the presence of a hard, absorbed component suggests the interaction of a high velocity flow interacting with a dense medium very close to the star.

A number of puzzles remain. The cause of the X-ray overluminosity of the WR star HD 93162 and the group of early B stars detected by the PSPC is unknown. In addition, while we confirm the existence of extended emission at a temperature of a few $\times 10^7$ K, we cannot constrain the physical origin of this gas. Observations of this region with broad-bandpass imaging spectrometers (such as those on ASCA) are needed in order to further explore these questions and to more fully probe the dynamics of the region as measured by the X-ray emission.

REFERENCES

Becker, R.H., Boldt, E.A., Holt, S.S., Pravdo, S.H., Rothschild, R.E., Serlemitsos, P.J., & Swank, J.H. 1976, ApJ, 209, L65
Chlebowski, T., Seward, F.D., Swank, J., & Szymkowiak, A. 1984, ApJ, 281, 665
Davidson, K. 1971, MNRAS, 154, 415
Forman, W., Jones, C., Cominsky, L., Julien, P., Murray, S., Peters, G., Tananbaum, H., & Giacconi, R. 1978, ApJS, 38, 357
Koyama, K., Asaoka, I., Ushimaru, N., Yamauchi, S., & Corbet, R.H.D. 1990, ApJ, 362, 215
Pollovk, A.M.T. 1987, ApJ, 320, 283
Seward, F.D., & Chlebowski, T. 1982, ApJ, 256, 530
Seward, F.D., Forman, W.R., Giacconi, R., Griffiths, R.E., Harnden Jr., F.R., Jones, C., & Pye, J.P. 1979, ApJ, 234, L55
Warren-Smith, R.F., Scarrott, S.M., Murdin, P., & Bingham, R.G. 1979, MNRAS, 187, 761